Balanced BPFs With Wideband CM Suppression and High Selectivity Based on Double-Sided Parallel-Strip Line

Hong-Yu Liu[1], Xing-Chen Zhou[1], Rui Li[1], Feng Wei[1]

E-mail: 23021211391@stu.xidian.edu.cn

1. National Key Laboratory of Radar Detection and Sensing, Xidian University, Xi'an, 710071, China.

ABSTRACT- In this paper, two novel balanced bandpass filters (BPFs) with wideband common-mode (CM) suppression and high selectivity are proposed based on the out-of-phase double-sided parallel strip-line (DSPSL) structure. The out-of-phase DSPSL structure is composed of a pair of out-of-phase transmission lines as the balanced ports and a λ/2 resonator placed in the center. Based on the DSPSL structure with out-of-phase characteristics, a wideband CM suppression without affecting the differential-mode (DM) performance is achieved in two BPFs. By using a pair of shorted-coupled lines in BPF I and introducing a ring resonator in BPF II, two transmission zeros are attained, achieving high selectivity in both BPF designs. For experimental demonstration purposes, two balanced BPFs are designed and fabricated. The measured results are in good agreement with the simulated ones.

Keywords: Balanced bandpass filter (BPF), common-mode (CM) suppression, double-sided parallel strip line (DSPSL), high selectivity.

1 INTRODUCTION

Bandpass filters (BPFs) with advanced performances are important passive components of modern radio frequency (RF) communication systems[1]-[4]. Moreover, balanced BPFs have attracted tremendous attention due to their high immunity to environmental noise and interference when compared with single-ended ones [5]-[8]. Recently, many balanced filters have been designed and analyzed [9]-[24].

Some balanced filters were designed based on symmetrical structure [11]-[14], which utilizes the symmetrical circuit topology at the central plane to achieve the short- and open-circuit characteristics under differential-mode (DM) and common-mode (CM) excitation, respectively.

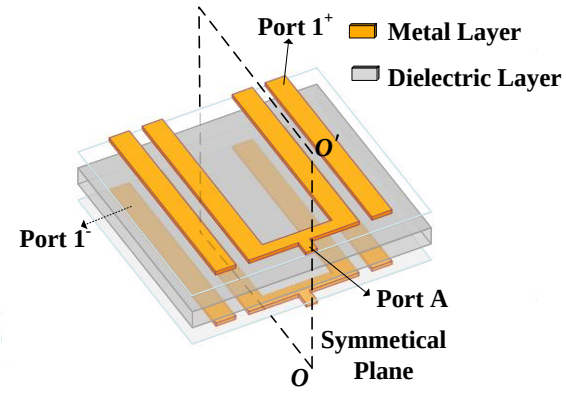

Fig. 1. 3-D diagram of the out-of-phase DSPSL structure.

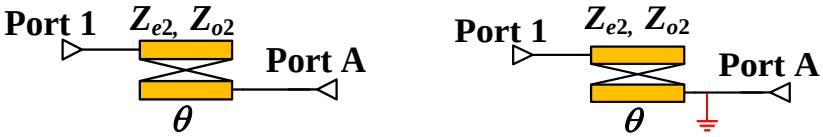

(a) (b)

Fig. 2. Equivalent circuits of the designed out-of-phase DSPSL structure. (a) DM simplified equivalent circuit. (b) CM simplified equivalent circuit.

However, for the above filters, the CM suppression is only implemented in a relatively narrow band or the size is relatively large. 180° swap structures based on double-sided parallel-strip line (DSPSL) were utilized to design balanced filters in [17] and [18], but the bandwidth of CM suppression is relatively limited.

Moreover, slotline-based balanced filters with wideband CM suppression have been reported recently [19]-[21]. Since the electric field distribution in the slotline conflicts with the magnetic wall's boundary condition, the CM signals would not transmit from the microstrip lines to the slotline and would be totally reflected. However, the DM selectivity of these designs needs to be further improved.

In this letter, an out-of-phase DSPSL structure is proposed for the design of balanced filters. In this structure, a pair of out-of-phase transmission lines is placed as the balanced ports and a λ/2 resonator is placed in the center. By designing the DSPSL structure with out-of-phase characteristics, a high level of wideband CM suppression without affecting the DM performance is obtained. Furthermore, this out-of-phase DSPSL structure is used to design two novel balanced BPFs. In these two BPFs, two additional transmission poles are attained by loading the shorted-loaded stubs in the coupled lines. A pair of shorted-coupled lines are used to attain two TZs for BPF I, and two TZs are produced by the ring resonator for BPF II. With

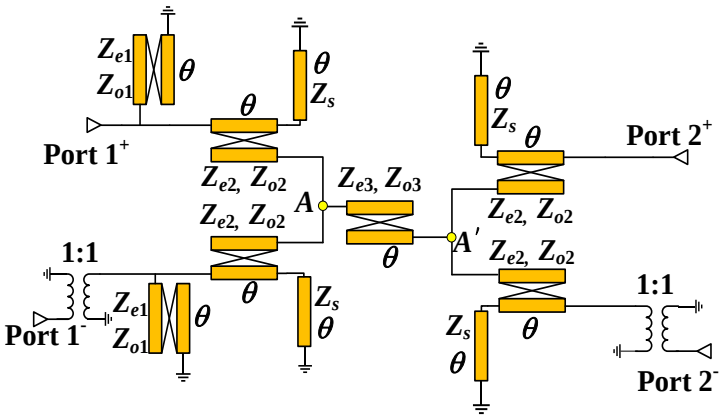

Fig. 3. Schematic diagram of the designed balanced BPF I.

the introduced close-to-band TZs, high selectivity is achieved in both two balanced BPFs.

2. THEORETICAL ANALYSIS and BALANCED BPF DESIGNS

In this section, the out-of-phase DSPSL structure is introduced in detail. Furthermore, two balanced BPFs with wideband CM suppression and high selectivity are designed based on the proposed out-of-phase DSPSL structure.

2.1 OUT-OF-PHASE DSPSL STRUCTURE

As shown in Fig. 1, the proposed out-of-phase DSPSL structure is composed of a pair of transmission lines with opposite phases as balanced ports and a λ/2 resonator placed in the center. By placing the balanced ports 1^+ and 1^- at the top layer and bottom layer, respectively, an intrinsic 180° phase shift between balanced ports 1^+ and 1^- is achieved [25]. Based on this out-of-phase design, when the balanced ports are excited by the DM signals, the phase of the DM signals will be turned from out-of-phase into in-phase, and a magnetic wall is generated at the symmetrical plane. However, when balanced ports are excited by the CM signals, the phase of the CM signals will be turned from in-phase into out-of-phase. Therefore, an electric wall is formed under the CM excitation, and the CM signals are suppressed.

Based on the above analysis, the simplified DM equivalent circuit and CM equivalent circuit of the out-of-phase DSPSL structure can be shown in Fig. 2(a) and (b). Under DM signals, the equivalent circuit is approximated as a coupled line (electrical length θ, even/odd-mode characteristic impedance Z_{e2}, Z_{o2}) and the resonance will occur at the center frequency f_0. Under CM excitation, the center of the λ/2 resonator is equivalent to a shorted point. Therefore, an approximate all-frequency CM suppression is obtained by applying the out-of-phase DSPSL

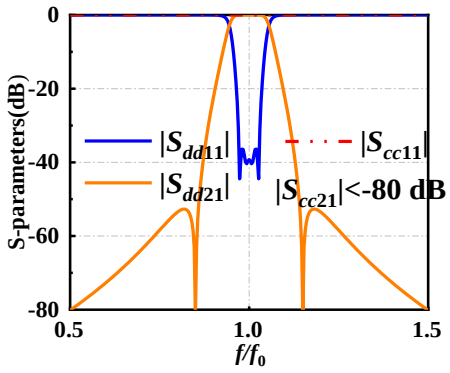

Fig. 4. (a) Calculated frequency responses of the proposed balanced BPF I (Z_{e1}=320 Ω, Z_{o1}=200 Ω, Z_{e2}=185 Ω, Z_{o2}=130 Ω, Z_{e3}=176 Ω, Z_{o3}=146 Ω, Z_s=61 Ω).

structure.

2.2 ANALYSIS of the DESIGNED BALANCED BPF I

The equivalent circuit of the designed balanced BPF I is shown in Fig. 3. In this letter, the schematic circuit of the 180° phase shift introduced by the out-of-phase DSPSL structure is represented by the transformer. A coupled line (electrical length θ, even/odd-mode characteristic impedance Z_{e3}, Z_{o3}) is located in the middle of two out-of-phase DSPSL structures, while the out-of-phase DSPSL structure is loaded with two shorted-loaded stubs (electrical length θ, characteristic impedance Z_s). Two shorted-coupled lines (electrical length θ, characteristic impedance Z_{e1}, Z_{o1}) are embedded in the input ports 1^+ and 1^-. The electrical length θ is set as 90° at f_0 = 1.7 GHz.

As discussed in part Sec. 2.1, when port 1^+ and port 1^- are excited by the CM signals, the phase of current on both sides of point A is inverted. Therefore, point A is equivalent to the shorted point under the CM excitation, and the CM signals cannot be further transmitted, achieving a wideband CM suppression.

When port 1^+ and port 1^- are excited by the DM signals, the out-of-phase signal will be changed to the in-phase signal at point A. The differential signals can be transmitted from the coupled line resonator to port 2.

The calculated DM and CM frequency responses of the proposed balanced BPF I are shown in Fig. 4. Two additional transmission poles are attained by the shorted-loaded stubs (θ, Z_s) [26]. Meanwhile, two close-to-band transmission zeros close to the operating frequency are introduced by the shorted-coupled lines, and a deeper roll-off rejection of the passband can be

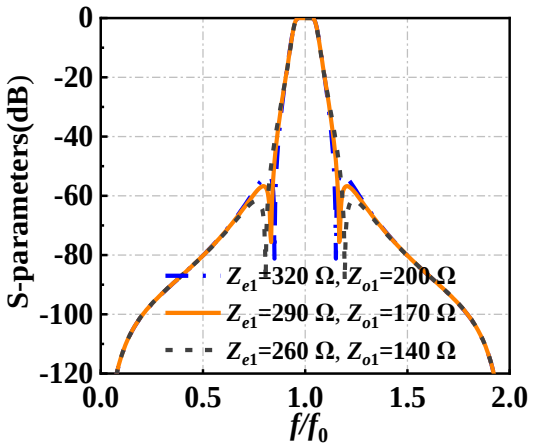

Fig. 5. $|S_{21}|$ analysis of balanced BPF I for various Z_{e1} and Z_{o1} (Z_{e2}=185 Ω, Z_{o2}=130 Ω, Z_{e3}=176 Ω, Z_{o3}=146 Ω, Z_s=61 Ω).

easily realized.

The shorted coupled lines produce two additional TZs, while two TZs can be studied by their input impedance (Z_{in}), and Z_{in} can be directly calculated as:

$$Z_{in} = \frac{j}{2}(Z_{e1} + Z_{o1})\tan\theta - \frac{j2Z_{e1}Z_{o1}}{(Z_{e1} + Z_{o1})\sin\theta\cos\theta} \tag{1}$$

When Z_{in} is equal to zero, two TZs can be obtained:

$$\theta_{TZ1} = \arcsin\left(\frac{2\sqrt{Z_{e1}Z_{o1}}}{(Z_{e1} + Z_{o1})}\right) \tag{2}$$

$$\theta_{TZ2} = \pi - \theta_{TZ1} \tag{3}$$

From the formulas (2) and (3), two TZs can be adjusted independently, which significantly improves the flexibility of the balanced circuit design. As shown in Fig. 5, the two close-to-passband TZs (f_{TZ1}, f_{TZ2}) change with different values of Z_{e1} and Z_{o1}.

Next, to improve the selectivity of the balanced BPF, another balanced BPF structure is designed. The ring resonator is placed in the middle of the two out-of-phase DSPSL structures instead of the coupled lines.

2.3 ANALYSIS OF THE DESIGNED BALANCED BPF II

The equivalent circuit of the designed balanced BPF II is shown in Fig. 6. A ring resonator is located in the middle of two out-of-phase DSPSL structures, and the out-of-phase DSPSL structure is loaded with two shorted-loaded stubs (electrical length θ, characteristic impedance Z_s). The ring resonator is composed of two open coupled lines (electric length θ, even/odd-mode characteristic impedance Z_{e3}, Z_{o3},) and two microstrip transmission lines (electric length

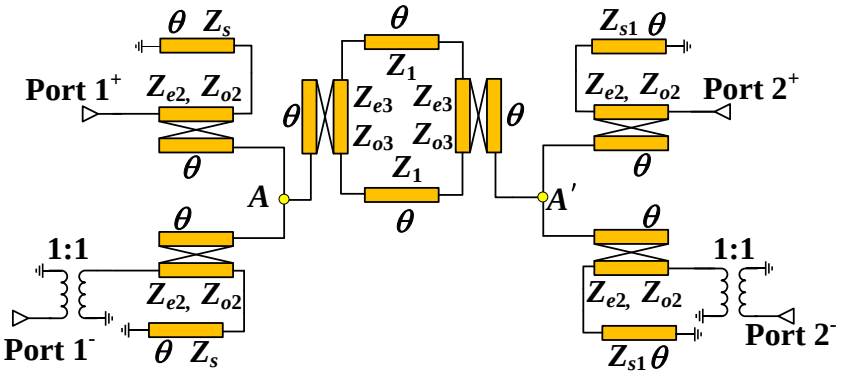

Fig. 6. Schematic diagram of the designed balanced BPF II.

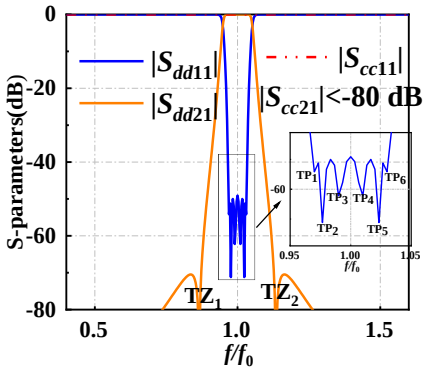

Fig. 7. Calculated frequency responses of the proposed balanced BPF II (Z_{e2}=187 Ω, Z_{o2}=132 Ω, Z_{e3}=164 Ω, Z_{o3}=124 Ω, Z_1=132 Ω, Z_s=100 Ω).

θ, characteristic impedance Z_1). The electrical length θ is set as 90° at f_0 = 1.7 GHz.

The calculated DM and CM frequency responses of the proposed balanced BPF II are given in Fig. 7. Wideband CM suppression can be achieved by the out-of-phase DSPSL structure. Two transmission zeros (TZ_1, TZ_2) and two transmission poles (TP_1 and TP_6) are produced by the ring resonator. The TP_3 and TP_4 are produced by the open coupled lines of the out-of-phase DSPSL structure. And the TP_2 and TP_5 are produced by the shorted-loaded stubs.

The equivalent circuit of the ring resonator can be analyzed with the ABCD matrices and which can be calculated as $M_o \times M_t \times M_o$, where M_o represents the open coupled lines (Z_{e3}, Z_{o3}), M_t represents the two middle transmission lines (Z_1), and M_o, M_t can be got from [27][28]. After further matrices conversions to S-parameters matrices, when S_{21} is equal to 0, we can obtain the following relationships:

$$\frac{(Z_{e3}+Z_{o3})^2+4Z_1(Z_{e3}+Z_{o3})+4Z_1^2}{(Z_{e3}+Z_{o3})^2}\cos^2\theta-\frac{(Z_{e3}+Z_{o3})^2-4Z_1^2}{(Z_{e3}+Z_{o3})^2}=0 \quad (4)$$

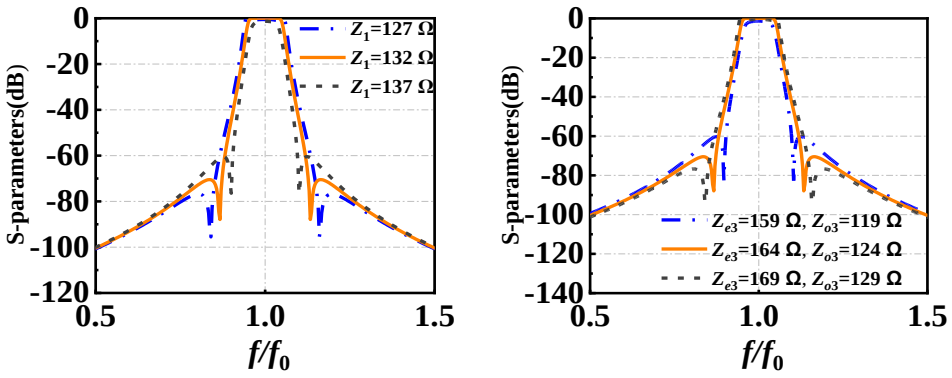

(a) (b)

Fig. 8. $|S_{21}|$ analysis of balanced BPF II for various Z_1, Z_{e3} and Z_{o3} (Z_{e2}=164 Ω, Z_{o2}=124 Ω, Z_1=132 Ω, Z_s=100 Ω). (a) $|S_{21}|$ for various Z_1 (Z_{e3} =164 Ω, Z_{o3} =124 Ω). (b) $|S_{21}|$ for various Z_{e2} and Z_{o2} (Z_1=132 Ω).

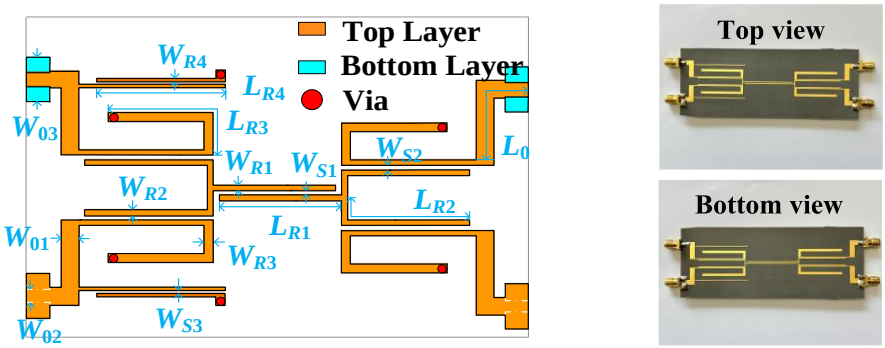

(a) (b)

Fig. 9. (a) Configuration of the proposed balanced BPF I. (Dimensions in mm: W_{R1} = 0.51, L_{R1} = 31.9, W_{R2} = 0.52, L_{R2} = 32.5, W_{R3} = 1.62, L_{R3} = 31.2, W_{R4} = 0.23, L_{R4} = 33.7, W_{s1} = 0.6, W_{s2} = 0.22, W_{s3} = 0.2, W_{01} = 3.1, W_{02} = 2.6, W_{03} = 8, L_0 = 13.2). (b) Photographs of balanced BPF I.

$$\theta_{TZ1} = \arccos\sqrt{\frac{Z_{e3}+Z_{o3}-2Z_1}{Z_{e3}+Z_{o3}+2Z_1}} \tag{5}$$

$$\theta_{TZ2} = \pi - \theta_{TZ1} \tag{6}$$

According to formulas (5) and (6), the two close-to-passband TZs are influenced by the values of the impedance value of Z_1. The varies of the TZs relatives to the different impedance values of Z_1 is shown in Fig 8(a). With the impedance Z_1 increases, two TZs move towards f_0. The influence of even/odd-mode characteristic impedance Z_{e3} and Z_{o3} are also given in Fig. 8(b), two TZs move close to the center frequency when the sum of Z_{e3} and Z_{o3} decreases. The 3-dB bandwidth increases as the sum of Z_{e3} and Z_{o3} increases.

3. EXPERIMENT RESULTS

To confirm the experimental viability, two balanced BPFs are designed and fabricated. The two balanced BPFs are designed on an F4BM substrate (relative dielectric permittivity εr = 2.2,

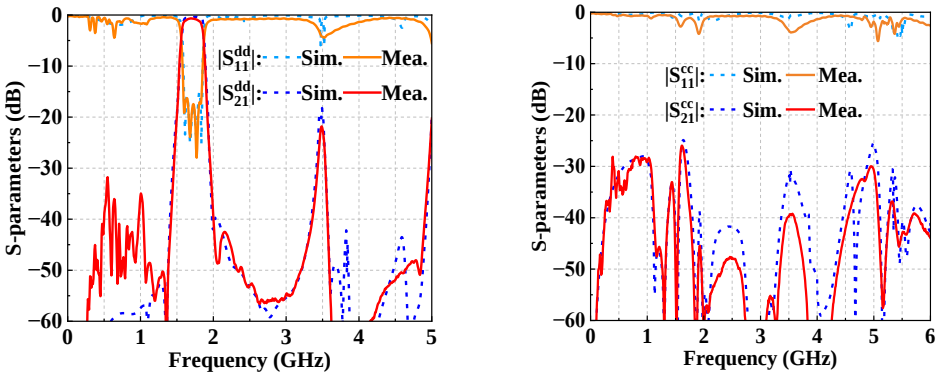

(a) (b)

Fig. 10. Simulation and measurement for the designed balanced BPF I. (a) DM responses. (b) CM responses.

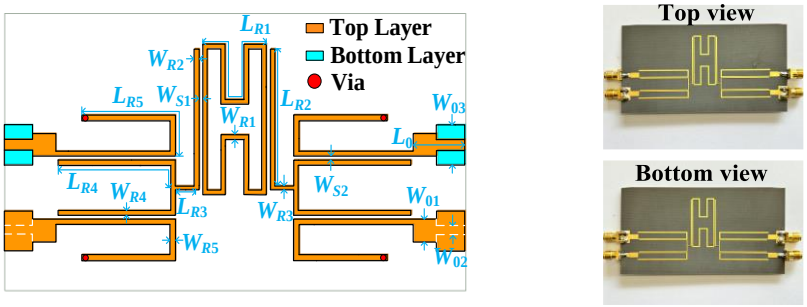

(a) (b)

Fig. 11. (a) Configuration of the proposed balanced BPF II. (Dimensions in mm: W_{R1} = 0.78, L_{R1} = 35.6, W_{R2} = 0.6, L_{R2} = 29.6, W_{R3} = 0.2, L_{R3} = 2, W_{R4} = 0.46, L_{R4} = 32.7, W_{R5} = 0.8, L_{R5} = 33.6, W_{s1} = 0.26, W_{s2} = 0.21, W_{01} = 3.1, W_{02} = 2.6, W_{03} = 8, L_0 = 10.5). (b) Photographs of balanced BPF II.

thickness H = 0.8 mm). The simulations are built by employing the commercial simulator Ansys HFSS 21.0, and measurements are obtained with the Agilent N5230A network analyzer.

The physical dimensions and photographs of the balanced BPF I are shown in Fig. 9 (a) and (b), respectively. The measured and simulated S-parameters of the designed balanced BPF I are shown in Fig. 10. The measured center frequency is at 1.71 GHz with the measured minimum insertion loss (IL) of 0.64 dB, and the 3-dB fractional bandwidth is 17.5%. The return loss is greater than 16.3 dB in the 3-dB fractional bandwidth. Meanwhile, the stopband reached up to 5.0 GHz (2.92 f_0) with a rejection level of 20 dB, and the AR_{20} which is defined in Table I is 283.3. Moreover, a suppression level over 26.1 dB can be achieved in all test bands (DC to 3.5 f_0) for the CM signals.

The physical dimensions and photographs of the balanced BPF II are shown in Fig. 11 (a) and (b), respectively. The measured and simulated S-parameters of the designed balanced BPF

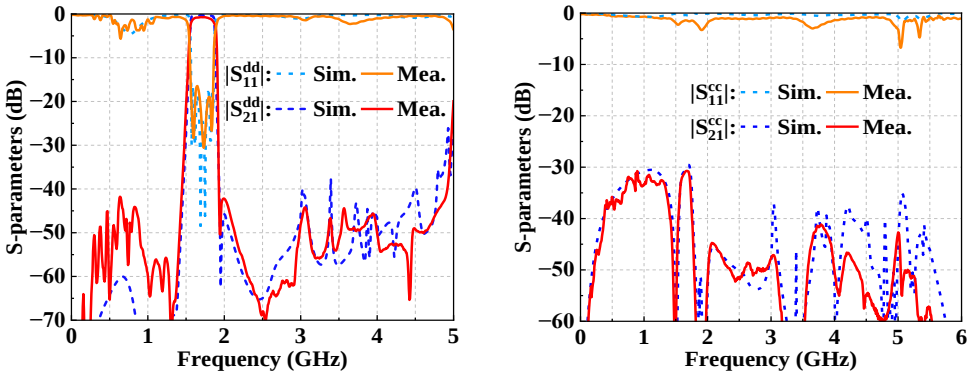

(a) (b)

Fig. 12. Simulations and measurements for the designed balanced BPF II. (a) DM responses. (b) CM responses.

TABLE I

COMPARISON BETWEEN DESIGNED WORKS AND OTHER WORKS

Ref.	f_0 (GHz)/ IL (dB)	3-dB FBW (%)/ AR_{20}	stopband (dB/GHz)	CMS (dB/GHz)
[4]	3/0.9	108/36.9	17.5/2.5f_0	/
[10]	5.7/0.85	12/113	30/1.58 f_0	34/1.58 f_0
[11]	5/1.7	67.6/26.15	15/2.7 f_0	15/1.6 f_0
[16]	2/0.5	12.9/106.25	25/1.875 f_0	20/1.42 f_0
[18]	2.2/1.8	23.6/154.5	20/2.91 f_0	20/2.9 f_0
Balanced BPF I	**1.71/0.64**	**17.5/283.3**	**20/2.92 f_0**	**26.1/≥3.5 f_0**
Balanced BPF II	**1.72/0.76**	**19.5/425**	**40/2.85 f_0**	**30.7/≥3.5 f_0**

IL: Insertion Loss; FBW: Fractional Bandwidth; CMS: CM Suppression;
AR_{20} is defined as:

$$AR_{20dB} = \frac{20-3}{|f_{20dB} - f_{3dB}|}(dB/GHz)$$

where, f_{20dB} denotes the 20-dB frequency point of insertion loss, and f_{3dB} denotes the 3-dB frequency point of insertion loss.

II are shown in Fig. 12. The measured center frequency is at 1.72 GHz with the measured minimum IL of 0.76 dB, and the 3-dB fractional bandwidth is 19.5%. The return loss is greater than 16.5 dB in the 3-dB fractional bandwidth. Meanwhile, the stopband reached up to 4.91GHz (2.85 f_0) with a rejection level of 40 dB, and the AR_{20} is 425. Moreover, a suppression level over 30.7 dB can be achieved in all test bands (DC to 3.5 f_0) for the CM signals.

Meanwhile, a comparison of two balanced BPFs with related prior-art designs is illustrated in Table I. Compared with former works [9], [12], [15], and [17], a wider band of CM

suppression is achieved in the proposed balanced BPFs. Moreover, the proposed balanced BPFs have higher AR_{20} and wider DM stopband with regard to [9], [12], [15], and [17].

4. CONCLUSION

In this letter, two balanced BPFs are proposed based on the proposed out-of-phase DSPSL structure. By designing the DSPSL structure with out-of-phase characteristics, a high level of wideband CM suppression without affecting the DM performance is obtained. And the close-to-band TZs of the two balanced BPFs are also analyzed. Wideband CM suppression, high selectivity, and wide stopband are achieved in both two balanced BPFs. Finally, two proposed designs have been manufactured. The measured and simulated results are presented with good agreement.

References

[1] J. Shi, J. Ren, J. Dong, W. Feng, and Y. Yang, "Supercompact Balanced Wideband Bandpass Filter Using Capacitor-Loaded Three-Line Coupled Structure," IEEE Microw. Wireless Compon. Lett, vol. 32, no. 6, pp. 499-502, June 2022.

[2] Y. -H. Zhu, J. Cai, and J. -X. Chen, "Quasi-Reflectionless Double-Sided Parallel-Strip Line Bandpass Filter With Enhanced Selectivity," IEEE Trans. Circuits Syst. II, Exp. Briefs, vol. 69, no. 2, pp. 339-343, Feb. 2022.

[3] Kai Da Xu, Zekai Luo, Yanhui Liu, Qing Huo Liu, "High-selectivity single-ended and balanced bandpass filters using ring resonators and coupled lines loaded with multiple stubs", AEU - International Journal of Electronics and Communications, vol. 96, 2018, Pages 193-198.

[4] W. Feng, W. Che and Q. Xue, "Compact DSPSL ultra-wideband bandpass filter based on transversal signal-interaction concepts," 2013 IEEE International Wireless Symposium (IWS), Beijing, China, 2013, pp. 1-4.

[5] Gang Xiong Wu, Yang Jin, Wei Zhang, Hao Wu, Ruirui Jiang, and Jin Shi, "Multi-functional balanced-to-single-ended filtering power divider with all-band output reflectionless and common-mode suppression", AEU - International Journal of Electronics and Communications, Volume 178, 2024,155266.

[6] Z. Tan, Q. -Y. Lu and J. -X. Chen, "Differential Dual-Band Filter Using Ground Bar-Loaded Dielectric Strip Resonators," IEEE Microw. Wireless Compon. Lett, vol. 30, no. 2, pp. 148-151, Feb. 2020.

[7] H. Zhu and Y. J. Guo, "Dual-Band and Tri-Band Balanced-to-Single Ended Power Dividers With Wideband Common-Mode Suppression," IEEE Trans. Circuits Syst. II, Exp. Briefs, vol. 68, no. 7, pp. 2332-2336, July 2021.

[8] H. -W. Deng, L. Sun, F. Liu, Y. -F. Xue, and T.2. Xu, "Compact Tunable Balanced Bandpass Filter With Constant Bandwidth Based on Magnetically Coupled Resonators," IEEE Microw. Wireless Compon. Lett, vol. 29, no. 4, pp. 264-266, April 2019.

[9] F. Wei et al., "Balanced Dual-Band BPF and FPD Using Quad-Mode RLR With Improved Selectivity," IEEE Trans. Circuits Syst. II, Exp. Briefs, vol. 69, no. 4, pp. 2081-2085, April 2022.

[10] Z. Zhang, G. Zhang, Z. Liu, W. Tang, and J. Yang, "Compact Balanced Bandpass Filter Based on Equilateral Triangular Patch Resonator," IEEE Trans. Circuits Syst. II, Exp. Briefs, vol. 69, no. 1, pp. 90-93, Jan. 2022.

[11] T. B. Lim and L. Zhu, "A Differential-Mode Wideband Bandpass Filter on Microstrip Line for UWB Application," IEEE Microw. Wireless Compon. Lett, vol. 19, no. 10, pp. 632-634, Oct. 2009.

[12] L. -L. Qiu, and Q. -X. Chu, "Balanced Bandpass Filter Using Stub-Loaded Ring Resonator and Loaded Coupled Feed-Line," IEEE Microw. Wireless Compon. Lett, vol. 25, no. 10, pp. 654-656, Oct. 2015.

[13] W. Feng, X. Gao, W. Che, W. Yang, and Q. Xue, "High Selectivity Wideband Balanced Filters With Multiple Transmission Zeros," IEEE Trans. Circuits Syst. II, Exp. Briefs, vol. 64, no. 10, pp. 1182-1186, Oct. 2017.

[14] X. Gao, W. Feng, and W. Che, "High-Selectivity Wideband Balanced Filters Using Coupled Lines With Open/Shorted Stubs," IEEE Microw. Wireless Compon. Lett, vol. 27, no. 3, pp. 260-262, March 2017.

[15] J. -X. Chen, Y. Zhan, W. Qin, Z. -H. Bao, and Q. Xue, "Novel Narrow-Band Balanced Bandpass Filter Using Rectangular Dielectric Resonator," IEEE Microw. Wireless Compon. Lett, vol. 25, no. 5, pp. 289-291, May 2015.

[16] Q. Liu, J. Wang, G. Zhang, L. Zhu, and W. Wu, “A New Design Approach for Balanced Bandpass Filters on Right-Angled Isosceles Triangular Patch Resonator,” IEEE Microw. Wireless Compon. Lett, vol. 29, no. 1, pp. 5-7, Jan. 2019.

[17] X. -H. Wang, Q. Xue, and W. -W. Choi, “A Novel Ultra-Wideband Differential Filter Based on Double-Sided Parallel-Strip Line,” IEEE Microw. Wireless Compon. Lett, vol. 20, no. 8, pp. 471-473, Aug. 2010.

[18] W. Feng, B. Pan, H. Zhu, X. Y. Zhou, W. Che, and Q. Xue, “High Performance Balanced Bandpass Filters With Wideband Common Mode Suppression,” IEEE Trans. Circuits Syst. II, Exp. Briefs, vol. 68, no. 6, pp. 1897-1901, June 2021.

[19] Y. -J. Lu, S. -Y. Chen, and P. Hsu, “A Differential-Mode Wideband Bandpass Filter With Enhanced Common-Mode Suppression Using Slotline Resonator,” IEEE Microw. Wireless Compon. Lett, vol. 22, no. 10, pp. 503-505, Oct. 2012.

[20] X. Guo, L. Zhu, and W. Wu, “Optimized Design of Differential Moderate-Band BPF on Coupled Slotline Resonators,” IEEE Microw. Wireless Compon. Lett, vol. 27, no. 3, pp. 263-265, March 2017.

[21] L. -P. Feng, and L. Zhu, “Strip-Loaded Slotline Resonator for Compact Differential-Mode Bandpass Filters with Improved Upper Stopband Performance,” IEEE Microw. Wireless Compon. Lett, vol. 27, no. 2, pp. 108-110, Feb. 2017.

[22] L. Yang, and R. Gómez-García, “High-Order Quasi-Elliptic-Type Single-Ended and Balanced Wideband Bandpass Filters Using Microstrip-to-Microstrip Vertical Transitions,” IEEE Trans. Circuits Syst. II, Exp. Briefs, vol. 70, no. 4, pp. 1425-1429, April 2023.

[23] Z. Li, F. Wei, B. Liu, and X. W. Shi, “Design of Balanced Wideband BPF Based on Tri-Mode Slotline Resonators,” IEEE Trans. Circuits Syst. II, Exp. Briefs, vol. 69, no. 6, pp. 2767-2771, June 2022.

[24] H. -W. Deng, T. Zhang, F. Liu, and T. Xu, “High Selectivity and CM Suppression Frequency-Dependent Coupling Balanced BPF,” IEEE Trans. Circuits Syst. II, Exp. Briefs, vol. 28, no. 5, pp. 413-415, May 2018.

[25] Y. Zhu, K. Song, M. Fan, S. Guo, Y. Zhou, and Y. Fan, “Common-Mode Noise Absorption Circuit Using Double-Sided Parallel-Strip Line,” IEEE Microwave and Wireless Components Letters, vol. 31, no. 1, pp. 25-28, Jan. 2021.

[26] T. H. Duong and I. S. Kim, “New Elliptic Function Type UWB BPF Based on Capacitively Coupled λ/4 Open T Resonator,” IEEE Transactions on Microwave Theory and Techniques, vol. 57, no. 12, pp. 3089-3098, Dec. 2009.

[27] H. -W. Deng, T. Zhang, F. Liu, and T. Xu, "High Selectivity and CM Suppression Frequency-Dependent Coupling Balanced BPF," IEEE Trans. Circuits Syst. II, Exp. Briefs, vol. 28, no. 5, pp. 413-415, May 2018.

[28] M. K. M. Salleh et al., “Quarter-wavelength side-coupled ring resonator for bandpass filters,” IEEE Trans. Microw. Theory Techn., vol. 56, no. 1, pp. 156–162, Jan. 2008.